Engineering with Computers (2020) 36:823–837
https://doi.org/10.1007/s00366-019-00733-0

ORIGINAL ARTICLE

Optimizing ANN models with PSO for predicting short building seismic response

Hoang Nguyen[1] · Hossein Moayedi[2,3] · Loke Kok Foong[4] · Husam Abdulrasool H. Al Najjar[5] · Wan Amizah Wan Jusoh[6] · Ahmad Safuan A. Rashid[4] · Jamaloddin Jamali[7]

Received: 12 January 2019 / Accepted: 4 March 2019 / Published online: 6 April 2019

Abstract
The present study aimed to optimize the artificial neural network (ANN) with one of the well-established optimization algorithms called particle swarm optimization (PSO) for the problem of ground response approximation in short structures. Various studies showed that ANN-based solutions are a reliable method for complex engineering problems. Predicting the ground surface respond to seismic loading is one of the engineering problems that still has not received any ANN solution. Therefore, this paper aimed to assess the application of hybrid PSO-based ANN models to the calculation of horizontal deflection of columns in short building after being subjected to a significant seismic loading (e.g., The Chi-Chi earthquake used as one of the input databases). To prepare both of the training and testing datasets, for the ANN and PSO-ANN network models, a series of finite element (FE) modeling were performed. The used FEM simulation database consists of 8324 training datasets and 2081 testing datasets that is equal to 80% and 20% of the whole database, respectively. The input includes Chi-Chi earthquake dynamic time (s), friction angle (φ), dilation angle (ψ), unit weight (γ), soil elastic modulus (E), Poisson's ratio (v), structure axial stiffness (EA), and bending stiffness (EI) where the output was taken horizontal deflection of the columns at their highest level (U_x). The result indicates higher reliability of the PSO-ANN model in estimating the ground response and horizontal deflection of structural columns in short structures after being subjected to earthquake loading.

Keywords ANN · Optimization · PSO-ANN · Earthquake · Short building

✉ Hossein Moayedi
hossein.moayedi@tdtu.edu.vn

[1] Institute of Research and Development, Duy Tan University, Da Nang 550000, Vietnam

[2] Department for Management of Science and Technology Development, Ton Duc Thang University, Ho Chi Minh City, Vietnam

[3] Faculty of Civil Engineering, Ton Duc Thang University, Ho Chi Minh City, Vietnam

[4] Center of Tropical Geoengineering, School of Civil Engineering, Faculty of Engineering, Universiti Teknologi Malaysia, 81310 Johor Bahru, Johor, Malaysia

[5] Centre for Advanced Modelling and Geospatial Information Systems (CAMGIS), Faculty of Engineering and IT, University of Technology Sydney, Sydney, NSW 2007, Australia

[6] Faculty of Engineering Technology (FTK), Universiti Tun Hussein Onn Malaysia, Campus (Pagoh Branch), Higher Education Hub Pagoh, KM1, Jalan Panchor, 84600 Pagoh, Muar, Johor, Malaysia

[7] College of Engineering and Technology, American University of the Middle East, Egaila, Kuwait

1 Introduction

Geotechnical earthquake engineering is recognized as the basis of civil engineering projects, so the study of ground response and its effect on the above structures is essential to soil mechanics and geotechnical engineering [1–6]. In addition, variation in soil properties beneath structures and complex geological structure (e.g., soil stiffness, soil-interface interactions, and structural elements) are important to consider into calculations [7–14]. Most traditional methods rely on complex solutions, i.e., using nonlinear seismic response analysis consideration [15] and extensive experimental methods [16]. In most cases, the proposed solutions illustrated how a specific ground motion affects the structures. In this regard, the structural deformations (e.g., located on a homogenous sandy soil layer) caused by earthquake loading have been proven a function in several key factors namely, ground characteristics [e.g., friction angle (φ), dilation angle (ψ), unit weight (γ), soil elastic modulus (E), Poisson's ratio (v)], structure characteristics [e.g., axial stiffness (EA) and

bending stiffness (EI)], and seismic loading (e.g., variation of ground acceleration/velocity/displacement versus dynamic time). Different equations have been developed to compute the horizontal deflection of structures (e.g., for a particular earthquake) (e.g., Hajikhodaverdikhana et al. [17], Men [18], Arulmoli et al. [19], Gulkan and Yazgan [20], Qu et al. [21] and Thomas et al. [22]). The main concern of computing the horizontal displacement of vertical structural elements (e.g., such as columns as used in this study) is to minimize its likelihood of high deformation after real seismic loadings were applied. The most influential factors in calculating a correct value for the seismic response of ground and its effect on structural deformations, i.e., maximum horizontal displacement of vertical columns, are (i) soil properties (e.g., soil stress–strain properties), (ii) structural stiffness (e.g., material properties and flexural stiffness of structural elements) and (iii) earthquake loading applied to the ground. Note that the soil characteristics such as internal friction angle and cohesion, dilation angle, unit weight, elastic modulus, Poisson's ratio as well as applied seismic loading on the above structures significantly affect the output.

In general, understanding the horizontal deformation of structures in a time of earthquake is a key factor in designing both short and high-rise buildings. For instance, different input parameters such as baseline material properties, foundation flexibility, and type of soil will influence the structural displacement. Numerous researchers such as Funck et al. [23], Pijush [24], Latifi et al. [25] and Uncuoglu [26] as well as Ahmadi and Kouchaki [27] have argued and introduced formulas to provide a reliable approximation of the horizontal deformation of short building structures. However, in reality, all these formulas are not reliable enough since they do not consider all influential parameters into their calculations. Artificial neural network (ANN) solutions are well introduced to support the prediction complex engineering problems [28–36] such as of horizontal displacement in structures built on single homogenous soil environments (e.g., Asadizadeh and Hossaini [37], Hasanzadehshooiili et al. [38], Gao and He [39]). In this study, to predict the maximum horizontal deformation of structures (maximum horizontal displacement at the highest level of columns) subjected to an earthquake (e.g., Chi-Chi earthquake), 84 different ANN models (6 iterations each with 14 different number of neurons) and 29 hybrid PSO-ANN models (e.g., helping the ANN to provide a better performance result) were designed.

2 FEM simulation and data collection

To determine horizontal deformation of the columns (U_x), i.e., subjected to the Chi-Chi earthquake (occurred in Taiwan on 21 September, 1999), we conducted a series of plane strain finite element modeling (FEM) for a building (e.g., a width equal to 1.0 m) located on a single layer soil (Fig. 1). In practical civil engineering projects, the soil layers beneath the building are usually not homogeneous; however, in most scenarios, a single layer of soil with uniform characteristics is used beneath the buildings. A commercial finite element software called Plaxis 2D was used to calculate the effects of earthquake loading on deformation of a short building (e.g., a four-level story) placed on a single sandy layer environment (Fig. 1a). Based on several recommendations (e.g., [40–54]), the most influential parameters that affect the maximum displacement of building columns are structural bending and axial stiffness as well as soil properties, [e.g., (i) friction angle (ϕ), (ii) dilation angle (ψ), (iii) unit weight(γ), (iv) elastic modulus (E), and (v) Poisson's ratio (υ)] (Table 1). It is important to note that cohesion was almost zero (e.g., the minimum possible value was equal to one as taken in the FEM) as the study aimed to predict the U_x in single-layered sandy soil. Needless to say that values of zero for cohesion (soil without any cohesive strength) supply sandy soil condition. Besides, values of H equal to 5 m were used for the distance between the columns. However, for each iteration, only one of the columns (shown in Fig. 2b) was considered. Ten different points (e.g., A–J) were selected as the target points where the maximum displacement occurred. Note that the displacement changes with time during the earthquakes. These changes were recorded for each point. For the dynamic loading, Chi-Chi 1999 in Taiwan, one of the most devastating recorded earthquakes was used. The variation of the acceleration versus time for the 1999 Chi-Chi, Taiwan, Earthquake is presented in Fig. 2. In this study, eight different sandy soils with a considerable difference in their basic characteristics were used in this study. These properties cover almost most of the common types of cohesionless soils. In terms of dilation angle and internal friction angle, ranges of 3.4–11.5° and 32–42° were considered and utilized in the modeling, respectively. In addition, the unit weight, elastic modulus and, Poisson's ratio varied between 19.0 and 21.1 kN/m^3, 17,500–65,000 kN/m^2 and 0.333–0.249, respectively. The properties of soils that were considered into network prediction (e.g., shown as a descriptive view of the range of input database) including unit weight, friction angle, elastic modulus, and Poisson's ratio are shown in Fig. 3. Figure 4 also presents the graphical summary and the range of input data (e.g., axial stiffness and bending stiffness of the structure) versus structural type. To ensure the rigidity of the columns at their lowest points, a rigid footing was considered at the bottom point of each column. Since the footing properties were not changed during the FEM simulations, thus it is not considered as one of the influential parameters.

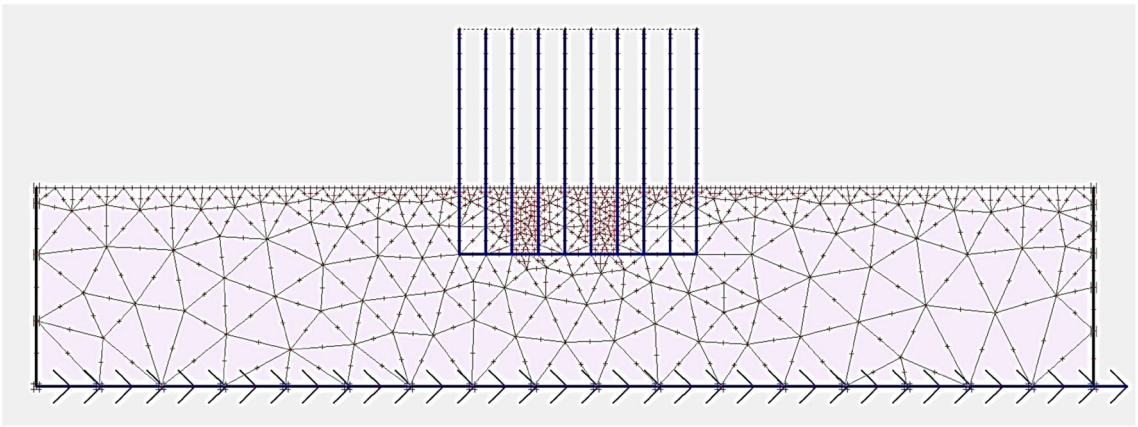

(a)

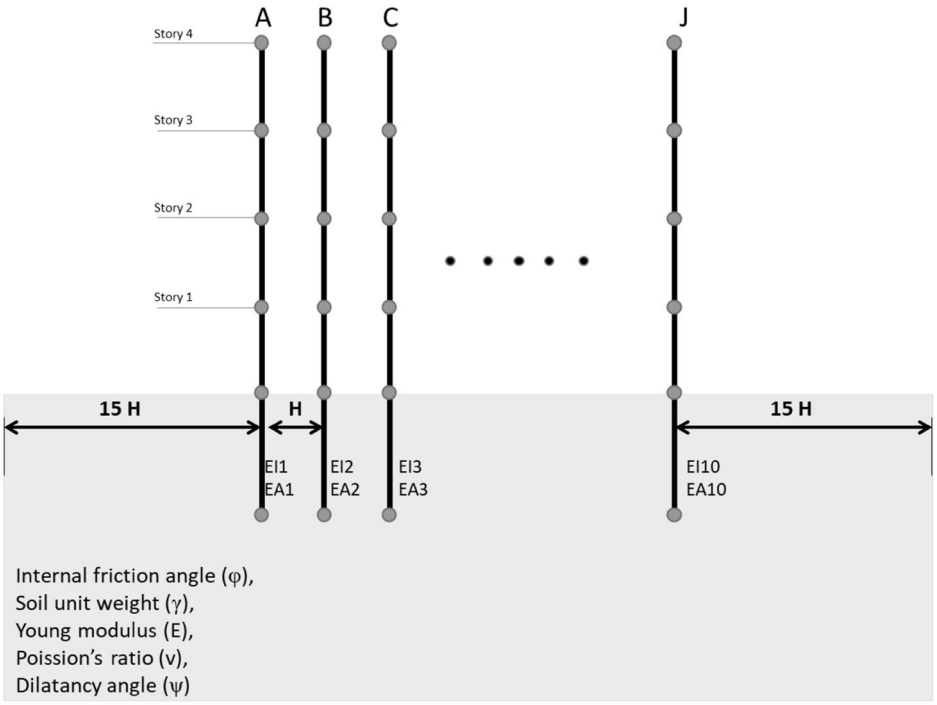

(b)

Fig. 1 A view of the model for the short building. **a** schematic model, **b** FEM model

3 Model development for distribution of building response estimation

The FEM simulation database that is used to train the ANN and PSO-ANN models were from a total of 10,403 full-scale models. The measured results from 8323 FEM calculations were chosen randomly to train the network. On the other hand, results from 2080 FEM simulations were used for the validation and testing datasets. The database provided for a short building with four stories rested on a single-layered soil condition. Note that the horizontal displacement values (U_x) varied with dynamic time (e.g., Chi-Chi time domain earthquake). In this study, the structural properties (e.g., column bending and axial stiffness), soil properties such as internal friction angle (φ), soil dilation angle (ψ), unit weight of the soil (γ), soil elastic modulus (E), and dynamic loading such as variation of acceleration with time (t)) selected as inputs and building response to earthquake (i.e., its deformation variation at their highest level) were taken as the output. A descriptive example of a database found from the FEM outputs and influential parameters affecting the U_x, as the model output, employed in ANN modeling is presented in Table 1.

Table 1 A small portion of the variables and database applied for modeling purpose

Input								Output
Time (s)	Friction angle (°)	Dilation angle (°)	Unit weight (kN/m^3)	Elastic modulus (kN/m^2)	Poisson's ratio (V)	Axial stiffness (EA)	Bending stiffness (EI)	U_x (m)
0.000	30	3.4	19	17,500	0.333	546,000	945	0.0127
0.000	30	3.4	19	17,500	0.333	546,000	945	0.0168
0.000	30	3.4	19	17,500	0.333	546,000	945	0.0175
20.930	31	4.2	19.3	20,000	0.327	546,000	945	0.0053
21.060	31	4.2	19.3	20,000	0.327	546,000	945	0.0054
21.190	31	4.2	19.3	20,000	0.327	546,000	945	0.0050
21.320	31	4.2	19.3	20,000	0.327	546,000	945	0.0043
21.450	31	4.2	19.3	20,000	0.327	546,000	945	0.0034
21.580	31	4.2	19.3	20,000	0.327	546,000	945	0.0022
21.710	31	4.2	19.3	20,000	0.327	546,000	945	0.0008
21.840	31	4.2	19.3	20,000	0.327	546,000	945	-0.0006
21.970	31	4.2	19.3	20,000	0.327	546,000	945	-0.0021
20.280	33	5.8	19.9	25,000	0.313	546,000	945	0.0020
20.410	33	5.8	19.9	25,000	0.313	546,000	945	0.0030
20.540	33	5.8	19.9	25,000	0.313	546,000	945	0.0036
15.080	37	8.8	20.7	40,000	0.285	4,158,000	121,128	-0.0014
15.210	37	8.8	20.7	40,000	0.285	4,158,000	121,128	0.0017
15.340	37	8.8	20.7	40,000	0.285	4,158,000	121,128	0.0053
15.470	37	8.8	20.7	40,000	0.285	4,158,000	121,128	0.0090
15.600	37	8.8	20.7	40,000	0.285	4,158,000	121,128	0.0128
15.730	37	8.8	20.7	40,000	0.285	4,158,000	121,128	0.0165
28.600	42	11.5	21.1	65,000	0.249	5,670,000	359,100	0.0730
28.730	42	11.5	21.1	65,000	0.249	5,670,000	359,100	0.0739
28.860	42	11.5	21.1	65,000	0.249	5,670,000	359,100	0.0747
28.990	42	11.5	21.1	65,000	0.249	5,670,000	359,100	0.0756
29.120	42	11.5	21.1	65,000	0.249	5,670,000	359,100	0.0764
29.250	42	11.5	21.1	65,000	0.249	5,670,000	359,100	0.0772

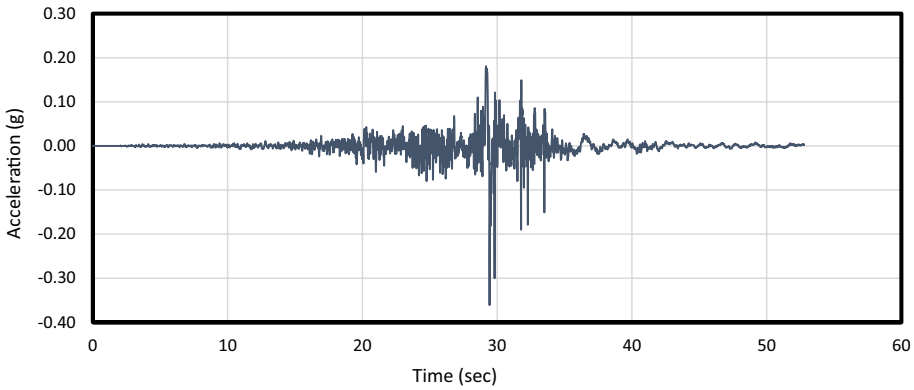

Fig. 2 Variation of acceleration (g) versus time (s) of the 1999 Chi-Chi, Taiwan, Earthquake (after Chang et al. [55])

4 Results and discussion

4.1 Measured building response

As stated earlier, short building structure was modeled on a single sandy soil layer. Note that the addition of soil layers will increase the complexity of the problem and multilayered baseline soil conditions are considered as the input database. To simplify the model, a single soil layer is modeled into the FEM calculations. Figure 5 presents the variation of the measured U_x versus time for two points of A and J. Note point A (e.g., highest elevation column no. 1) and point J

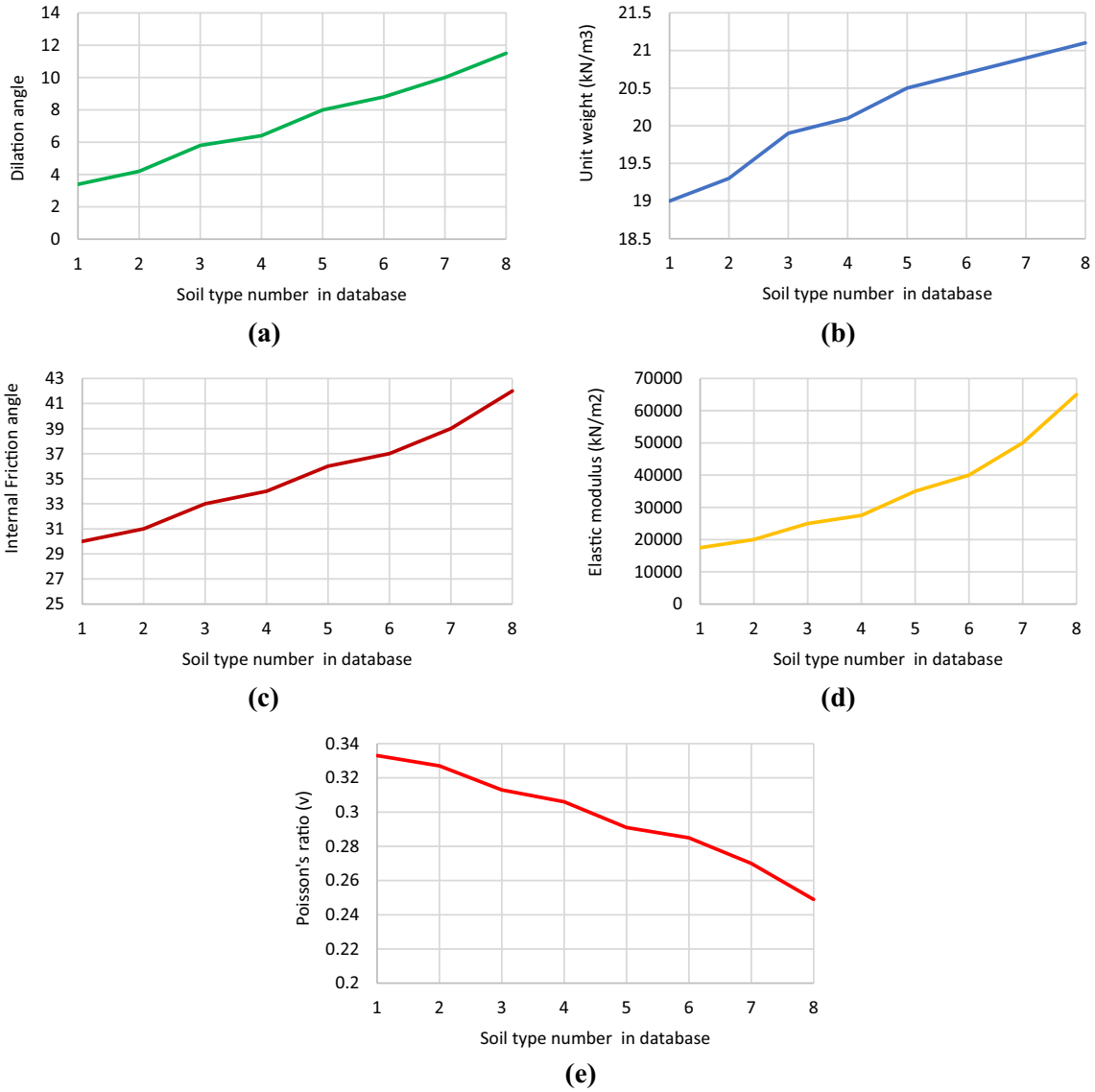

Fig. 3 Range of input data versus soil type (shown as a graphical summary)

(e.g., column no. 10). Note that column no. 1 (with point A at its highest level) had the minimum stiffness values where column no. 10 (with point J at its highest level) had the maximum stiffness values. From this figure, it can be seen that point A in column no. 1, (e.g., the most flexible case) the column itself will have fluctuated behaviors rather than a rigid case (e.g., point J) with a smooth deformation.

4.2 Artificial neural network

The use of the artificial neural network in finding a solution for the highly complex problem is well established [56–59]. In this study, prediction of the short building response to earthquake loading [i.e., shown as the horizontal deflection of the columns at their highest level (U_x)] is the aim of the current study. As in the first step of the ANN optimization, different testing and training datasets were considered for the proposed models. During the calculation process, we separated two datasets including 80% of the whole dataset for the training dataset and 20% of the whole dataset for the testing dataset. The best structure of the ANN model found after some trial and error processes and by varying the number of neurons and the number of hidden layers [60–66]. In this regard, we built a total of 84 ANN-Tansig models. The performance of proposed networks was measured to assess their best network outputs. As a final result, we presented the average result from six different ANN model iterations in Tables 2 and 3, for the network performance R^2 and RMSE, respectively. Two different ranking systems of total and color intensity ranking were used to rank the obtained

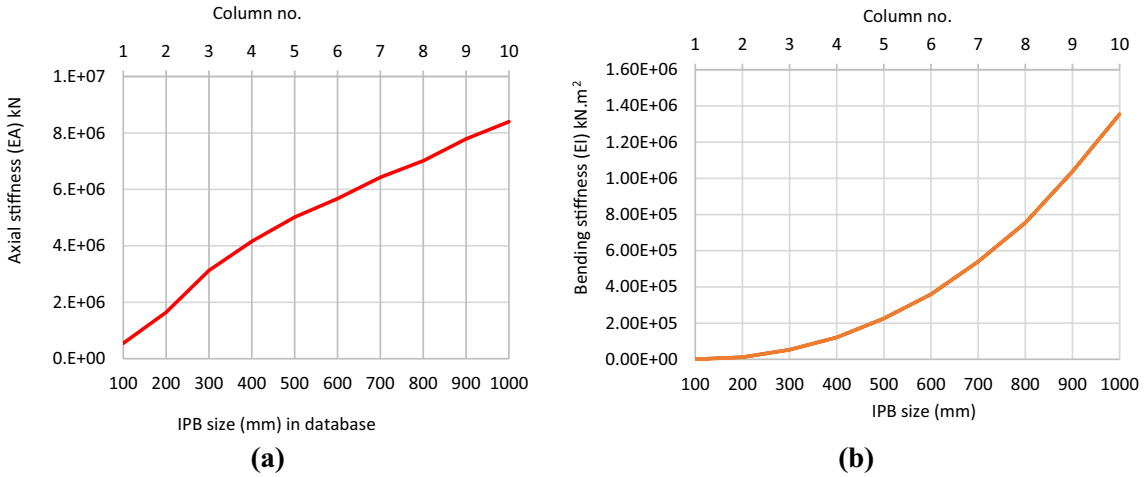

Fig. 4 A graphical description of input data for the structural type

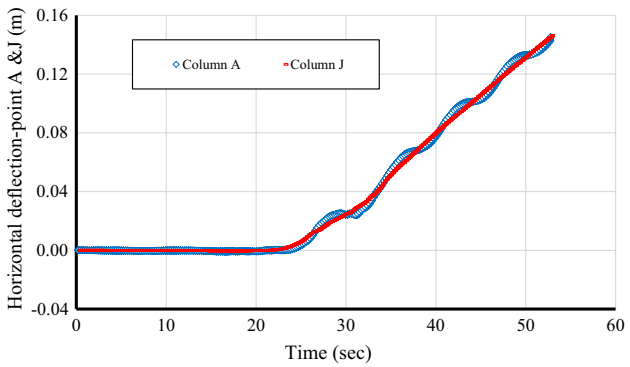

Fig. 5 Variation of the measured U_x versus time for point A in column no. 1 and point J in column no. 10. Note that column A has the minimum stiffness where column J has the maximum stiffness

outputs from the ANN modeling. Based on the average network result from all 84 ANN constructed networks (i.e., from both of the testing and the training datasets), the proposed model with the highest total ranking values (i.e., 27 and 28 on the R^2 and RMSE results, respectively) should designate as the best constructed model. However, after checking all network performance (as illustrated in Figs. 6, 7), the ANN model with eight hidden neurons in a single hidden layer resulted in a better network prediction result. This means the final ANN structure that was chosen for this model should have an $8 \times 12 \times 1$ structure but looking to the small changes in the network performance (as shown in Figs. 6, 7, respectively), the optimum value for the pre-defined number of nodes in a single hidden layer structure can be chosen to be four. In the case of this study and without simplification the best ANN structure for the calculation of the building response to earthquake loading was chosen to be $8 \times 12 \times 1$.

4.3 Hybrid PSO-ANN models

To measure the capability of both ANN and PSO-ANN methods, two ranking techniques were utilized (Table 4). These rankings are described well in other studies (e.g., Moayedi and Hayati [67], Moayedi et al. [68], Moayedi and Rezaei [69]). The accuracy results (i.e., shown by statistical indexes of R^2 and RMSE) for different values used for PSO influential parameter such as (i) population sizes, (ii) values considered for the acceleration constants of C_1 and C_2 and (iii) values between 0.2 and 1.0 that are considered for the term called inertia weight are presented in Figs. 8, 9, and 10, respectively. From these figures, it can be seen that the network performance (i.e., based on PSO-ANN model) that used swarm size equal to 400 (e.g., the swarm size that obtained the maximum total ranking), and both of the acceleration constants of C_1 and C_2 is equal to 2.0 (also in Table 5), respectively. Note that the inertia weight equal to 1.0 (Table 6) leads to the most reliable and accurate predictive PSO-ANN model.

Based on the obtained results, although all proposed models have satisfactory approximation results in estimation U_x, the proposed hybrid PSO-ANN model can be presented as a more reliable and better ANN model in this field. Almost in all predictive models, the learning process was acceptable. Figure 11 shows the results of RMSE for different acceleration constants and inertia weight. Based on R^2, RMSE and VAF, values of (0.9997, 0.0170 and 99.9293) and (0.9997, 0.0168 and 99.9950) are obtained for randomly selected training and testing of the proposed PSO-ANN models, respectively. Similarly, in ANN, the R^2, RMSE, and VAF for both of the training and the testing datasets were (0.99961, 0.01815 and 99.713) and (0.99963, 0.01748 and 99.720), respectively. From all presented models, the PSO-ANN predictive model can provide higher performance

Table 2 R^2 outputs for 84 proposed ANN models with a change in the hidden neurons for the estimation U_x

Model number	Nodes in the hidden layer	Network result																
		R^2																
		Iteration 1		Iteration 2		Iteration 3		Iteration 4		Iteration 5		Iteration 6		Average		Average Ranking		Total ranking
		TR1	TS1	TR2	TS2	TR3	TS3	TR4	TS4	TR5	TS5	TR6	TS6	TR	TS	TR	TS	
1	1	0.99815	0.99807	0.99810	0.99829	0.99815	0.99809	0.99811	0.99826	0.99818	0.99795	0.99812	0.99821	0.99814	0.99814	1	1	2
2	2	0.99944	0.99939	0.99944	0.99940	0.99944	0.99940	0.99943	0.99944	0.99835	0.99837	0.99893	0.99891	0.99917	0.99915	2	2	4
3	3	0.99954	0.99950	0.99943	0.99949	0.99946	0.99937	0.99944	0.99941	0.99889	0.99875	0.99944	0.99940	0.99937	0.99932	3	3	6
4	4	0.99944	0.99943	0.99952	0.99956	0.99944	0.99946	0.99953	0.99957	0.99947	0.99937	0.99958	0.99959	0.99950	0.99950	5	5	10
5	5	0.99960	0.99959	0.99942	0.99948	0.99944	0.99946	0.99945	0.99936	0.99954	0.99950	0.99951	0.99956	0.99949	0.99949	4	4	8
6	6	0.99953	0.99960	0.99953	0.99959	0.99954	0.99953	0.99960	0.99955	0.99955	0.99942	0.99956	0.99957	0.99955	0.99954	8	6	14
7	7	0.99955	0.99960	0.99955	0.99952	0.99955	0.99950	0.99952	0.99952	0.99963	0.99966	0.99963	0.99964	0.99957	0.99957	11	10	21
8	8	0.99967	0.99966	0.99954	0.99956	0.99961	0.99959	0.99954	0.99958	0.99952	0.99955	0.99943	0.99948	0.99955	0.99957	7	9	16
9	9	0.99959	0.99961	0.99954	0.99956	0.99958	0.99960	0.99943	0.99944	0.99958	0.99955	0.99959	0.99961	0.99955	0.99956	6	7	13
10	10	0.99961	0.99963	0.99979	0.99980	0.99960	0.99958	0.99944	0.99945	0.99970	0.99971	0.99978	0.99977	0.99965	0.99966	13	14	27
11	11	0.99955	0.99952	0.99957	0.99963	0.99961	0.99962	0.99954	0.99949	0.99981	0.99983	0.99985	0.99985	0.99965	0.99966	14	13	27
12	12	0.99961	0.99960	0.99956	0.99954	0.99944	0.99947	0.99954	0.99952	0.99953	0.99955	0.99974	0.99977	0.99957	0.99957	10	11	21
13	13	0.99960	0.99957	0.99962	0.99957	0.99958	0.99961	0.99943	0.99951	0.99959	0.99956	0.99954	0.99955	0.99956	0.99956	9	8	17
14	14	0.99963	0.99962	0.99961	0.99964	0.99961	0.99956	0.99955	0.99946	0.99965	0.99966	0.99977	0.99974	0.99964	0.99961	12	12	24

Table 3 RMSE outputs for 84 proposed ANN (LM) models with a change in the hidden neurons for the estimation U_x

Model number	Nodes in the hidden layer	Network result														Average Ranking		Total ranking
		RMSE																
		Iteration 1		Iteration 2		Iteration 3		Iteration 4		Iteration 5		Iteration 6		Average				
		TR1	TS1	TR2	TS2	TR3	TS3	TR4	TS4	TR5	TS5	TR6	TS6	TR	TS	TR	TS	
1	1	0.03926	0.03984	0.03968	0.03810	0.03925	0.03984	0.03925	0.03984	0.03911	0.04043	0.03948	0.03898	0.03934	0.03951	1	1	2
2	2	0.02160	0.02233	0.02161	0.02236	0.02157	0.02242	0.02157	0.02242	0.03708	0.03693	0.02995	0.02994	0.02557	0.02607	2	2	4
3	3	0.01958	0.01998	0.02183	0.02080	0.02141	0.02260	0.02141	0.02260	0.03039	0.03224	0.02152	0.02266	0.02269	0.02348	3	3	6
4	4	0.02169	0.02178	0.01992	0.01943	0.02162	0.02122	0.02162	0.02122	0.02107	0.02293	0.01873	0.01867	0.02077	0.02087	4	4	8
5	5	0.01835	0.01839	0.02195	0.02071	0.02159	0.02130	0.02159	0.02130	0.01950	0.02087	0.02024	0.01922	0.02054	0.02030	5	5	10
6	6	0.01979	0.01822	0.01972	0.01875	0.01942	0.02008	0.01942	0.02008	0.01934	0.02161	0.01911	0.01913	0.01947	0.01964	6	6	12
7	7	0.01923	0.01868	0.01943	0.02016	0.01944	0.02056	0.01944	0.02056	0.01754	0.01705	0.01750	0.01716	0.01876	0.01903	10	7	17
8	8	0.01644	0.01688	0.01951	0.01919	0.01786	0.01889	0.01786	0.01889	0.02007	0.01928	0.02180	0.02096	0.01892	0.01901	8	8	16
9	9	0.01853	0.01797	0.01965	0.01882	0.01876	0.01810	0.01876	0.01810	0.01869	0.01927	0.01850	0.01826	0.01882	0.01842	9	11	20
10	10	0.01815	0.01748	0.01329	0.01301	0.01826	0.01857	0.01826	0.01857	0.01584	0.01536	0.01358	0.01346	0.01623	0.01608	14	14	28
11	11	0.01937	0.01969	0.01892	0.01770	0.01808	0.01793	0.01808	0.01793	0.01246	0.01197	0.01115	0.01127	0.01634	0.01608	13	13	26
12	12	0.01802	0.01826	0.01911	0.01934	0.02172	0.02094	0.02172	0.02094	0.01984	0.01936	0.01479	0.01416	0.01920	0.01883	7	10	17
13	13	0.01837	0.01885	0.01782	0.01897	0.01850	0.01840	0.01850	0.01840	0.01853	0.01903	0.01953	0.01946	0.01854	0.01885	11	9	20
14	14	0.01764	0.01786	0.01798	0.01711	0.01806	0.01892	0.01806	0.01892	0.01716	0.01701	0.01378	0.01460	0.01711	0.01740	12	12	24

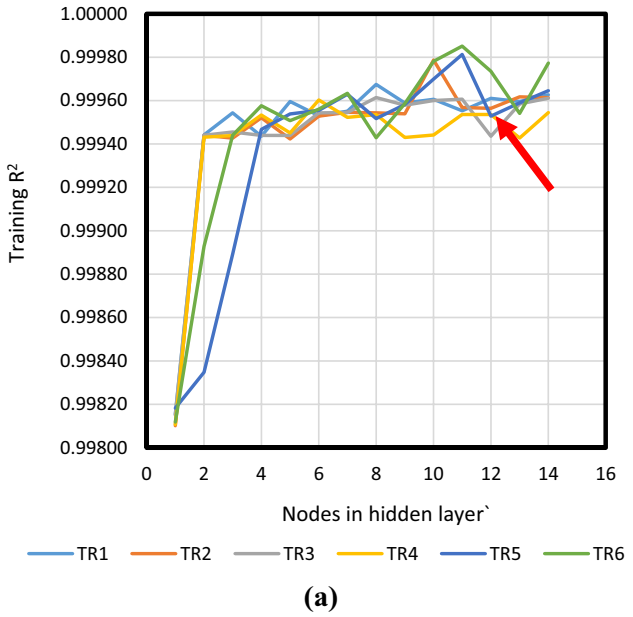

Fig. 6 R^2 outputs for 84 proposed ANN models with a change in the hidden neurons for the estimation U_x

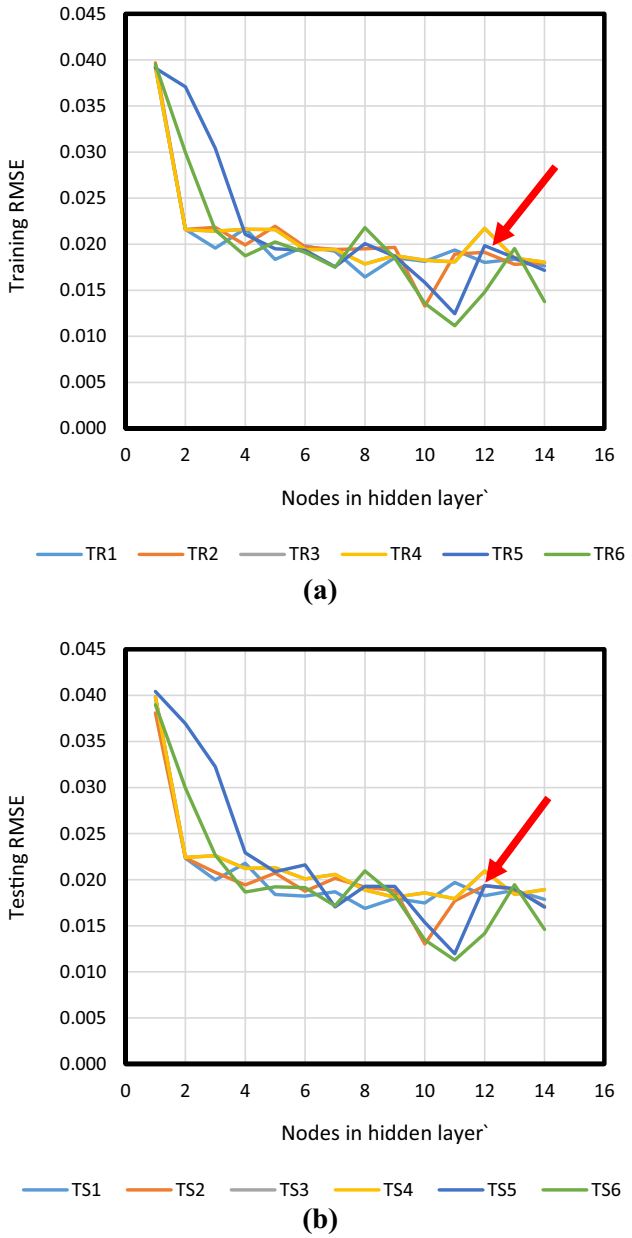

Fig. 7 RMSE outputs for 84 proposed ANN models with a change in the hidden neurons for the estimation U_x

results regarding all statistical indices (e.g., RMSE, $R^{2,}$ and VAF) for both training and testing phases compared to the other two methods. Training and testing results of the ANN model in predicting U_x based on the ANN predictive model (e.g., with ten nodes) and PSO-ANN predictive models are presented in Figs. 12 and 13, respectively. This ANN-based equation with the $8\times4\times1$ structure represents a reliable estimation model in predicting F_{ult}. This equation along with the proposed PSO-ANN structure showed excellent convergence as predictive networks (Eq. 1).

$$F_{\text{ult}} = \begin{pmatrix} (9.5121\times Y_1) + (0.2299\times Y_2) + (-7.7751\times Y_3) \\ +(8.0928\times Y_4) + (-0.0512\times Y_5) + (-0.5861\times Y_6) \\ +(0.4709\times Y_7) + (0.0545\times Y_8) + (0.1161\times Y_9) \\ +(0.0158\times Y_{10}) + (8.9937\times Y_{11}) + (-2.4076\times Y_{12}) + (-1.4402) \end{pmatrix}, \quad (1)$$

Table 4 PSO-ANN network results for different population sizes

Model number	Swarm size	Network result						Ranking						Total rank
		Train			Test			Train			Test			
		R^2	RMSE	VAF	R^2	RMSE	VAF	R^2	RMSE	VAF	R²	RMSE	VAF	
1	25	0.999642	0.017304	99.934	0.999607	0.01819	99.96	9	8	10	6	6	6	45
2	50	0.999603	0.018233	99.9214	0.999556	0.01902	99.96	6	6	5	1	3	2	23
3	75	0.999641	0.01724	99.9236	0.999621	0.01799	99.96	8	9	7	8	8	8	48
4	100	0.999802	0.012855	99.9580	0.999779	0.01358	99.98	12	12	12	11	11	11	69
5	150	0.99958	0.018768	99.9222	0.999584	0.0185	99.9	5	4	6	5	5	5	30
6	200	0.999553	0.019249	99.9089	0.999567	0.01928	99.963	2	2	1	2	1	3	11
7	250	0.999577	0.018751	99.913	0.999624	0.01786	99.96	4	5	4	9	9	9	40
8	300	0.999544	0.019662	99.9093	0.99962	0.01801	99.96	1	1	2	7	7	7	25
9	350	0.999564	0.018991	99.9119	0.999577	0.01909	99.96	3	3	3	4	2	4	19
10	400	0.999772	0.013782	99.9555	0.999779	0.01353	99.98	11	11	11	12	12	12	69
11	450	0.999659	0.016928	99.9309	0.999643	0.01729	99.970	10	10	9	10	10	10	59
12	500	0.999635	0.017514	99.9283	0.999569	0.0188	99.946	7	7	8	3	4	1	30

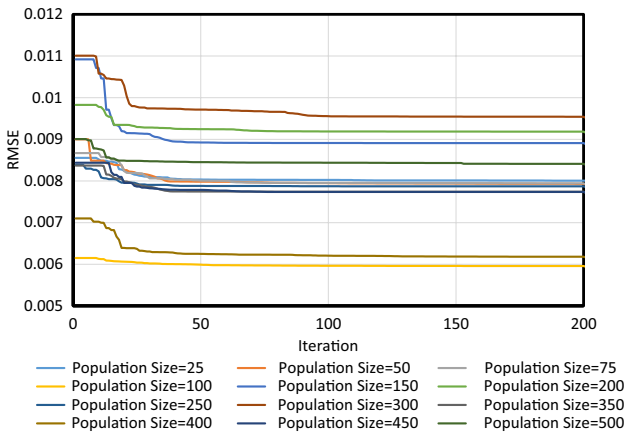

Fig. 8 The results of network performance for various population sizes

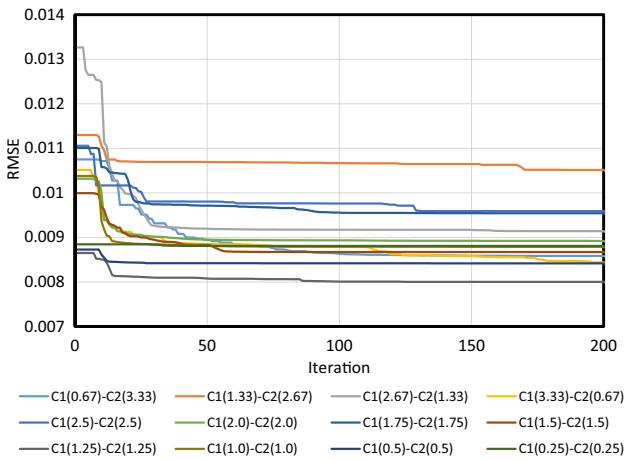

Fig. 9 Performance results for different C_1 and C_2 values

where

$$Y1 = \text{Tansig}(1.6090 \times A + (0.1264) \times B + (-0.0121) \times C + (2.0575)) \quad (2)$$

$$Y2 = \text{Tansig}(3.6824 \times A + (-0.5746) \times B + (-0.5475) \times C + (-1.4195)) \quad (3)$$

$$Y3 = \text{Tansig}(-5.1603 \times A + (-1.2555) \times B + (-0.4726) \times C + (-8.9539)) \quad (4)$$

$$Y4 = \text{Tansig}(-5.6652 \times A + (-1.1423) \times B + (-0.4409) \times C + (-13.7946)) \quad (5)$$

$$Y5 = \text{Tansig}(1.6469 \times A + (0.9256) \times B + (0.6186) \times C + (0.3377)) \quad (6)$$

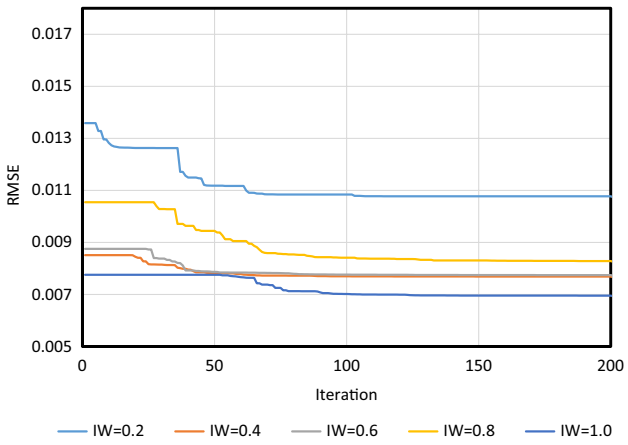

Fig. 10 Performance results for different inertia weight values

Table 5 PSO-ANN network results for different C_1 and C_2

Model number	C_1	C_2	Network result						Ranking						Total rank
			Train			Test			Train			Test			
			R^2	RMSE	VAF	R^2	RMSE	VAF	R^2	RMSE	VAF	R^2	RMSE	VAF	
1	0.67	3.33	0.999589	0.01862	99.918	0.999519	0.01961	99.959	10	10	10	1	2	2	35
2	1.33	0.67	0.999556	0.019292	99.910	0.999618	0.01801	99.967	6	5	6	10	9	10	46
3	2.67	1.34	0.999533	0.019779	99.905	0.999524	0.02046	99.960	2	2	1	2	1	3	11
4	3.33	0.67	0.999552	0.019512	99.908	0.999578	0.01885	99.964	4	4	4	5	5	6	28
5	2.50	2.50	0.999522	0.020004	99.907	0.999587	0.0184	99.965	1	1	3	7	7	8	27
6	2.00	2.00	0.999771	0.013875	99.95	0.999799	0.01291	99.983	12	12	12	12	12	12	72
7	1.75	1.75	0.999541	0.019615	99.905	0.999583	0.01886	99.965	3	3	2	6	4	7	25
8	1.50	1.50	0.999568	0.019027	99.914	0.999571	0.01884	99.964	9	9	9	4	6	5	42
9	1.25	1.25	0.999639	0.017348	99.925	0.999653	0.01714	99.97	11	11	11	11	11	11	66
10	1.00	1.00	0.999555	0.019244	99.912	0.999551	0.01951	99.962	5	6	8	3	3	4	29
11	0.50	0.50	0.999562	0.019112	99.91	0.999612	0.01824	99.967	8	8	7	8	8	9	48
12	0.25	0.25	0.99956	0.019216	99.909	0.999618	0.01766	99.939	7	7	5	9	10	1	39

Table 6 PSO-ANN network results for different inertia weight

Model number	Inertia weight	Network result						Ranking						Total rank
		Train			Test			Train			Test			
		R^2	RMSE	VAF	R^2	RMSE	VAF	R^2	RMSE	VAF	R^2	RMSE	VAF	
1	0.2	0.9995	0.0217	99.9090	0.9995	0.0210	99.9573	1	1	1	2	1	1	7
2	0.4	0.9996	0.0178	99.9196	0.9996	0.0187	99.9663	3	3	4	3	3	3	19
3	0.6	0.9996	0.0178	99.9178	0.9996	0.0181	99.9672	4	4	3	4	4	4	23
4	0.8	0.9995	0.0194	99.9144	0.9995	0.0199	99.9608	2	2	2	1	2	2	11
5	1.0	0.9997	0.0170	99.9293	0.9997	0.0168	99.9950	5	5	5	5	5	5	30

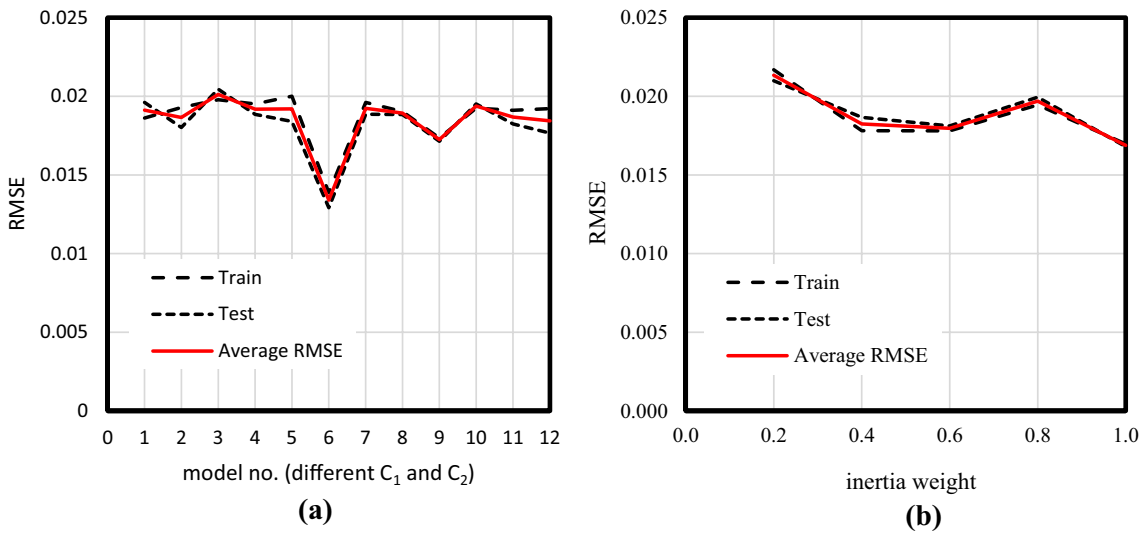

Fig. 11 RMSE results for different **a** acceleration constants and **b** inertia weight

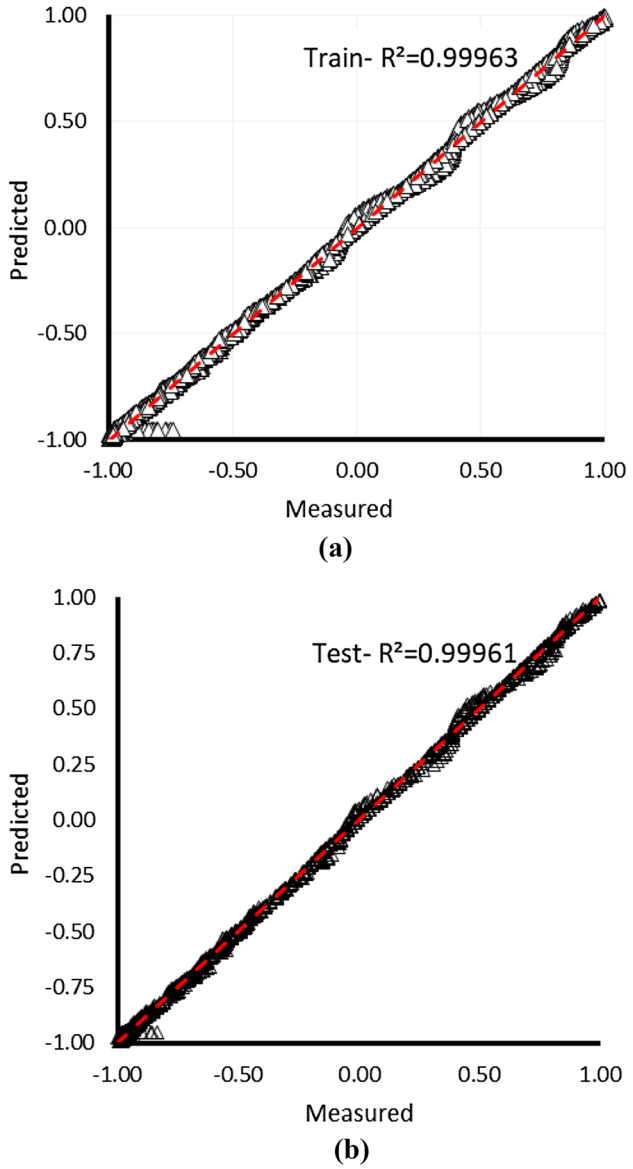

Fig. 12 Training and testing results of the ANN model in predicting F_{ult} (e.g., with ten nodes)

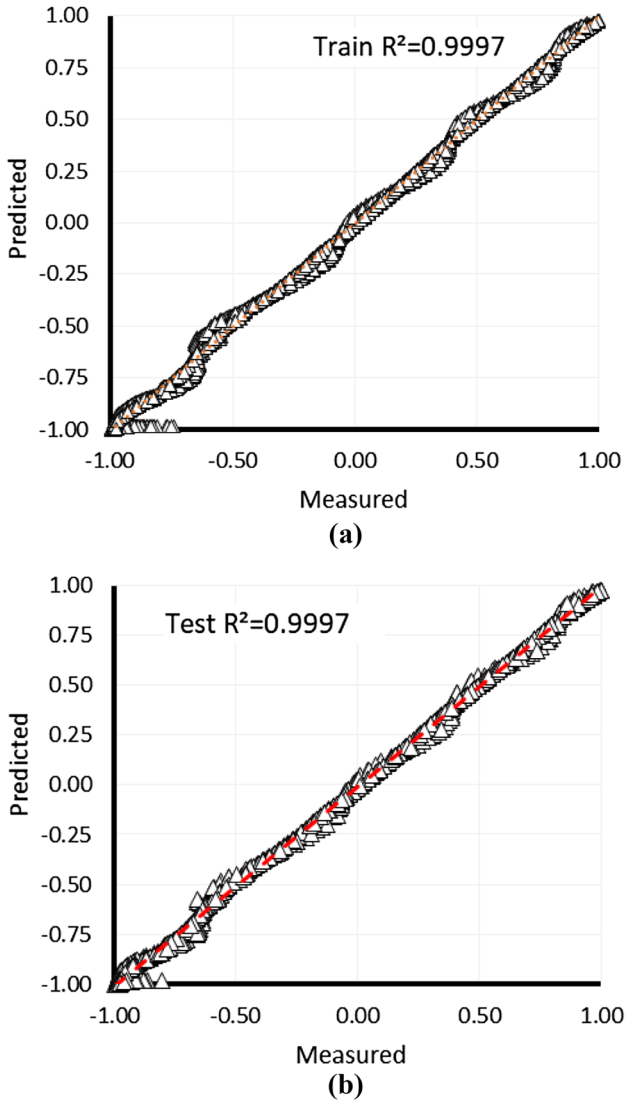

Fig. 13 Training and testing results of the PSO-ANN model in predicting F_{ult}

$$Y6 = \text{Tansig}(0.5167 \times A + (-0.1137) \times B + (-0.1865) \times C + (-0.6806)) \quad (7)$$

$$Y7 = \text{Tansig}(-4.7088 \times A + (0.4517) \times B + (-0.0639) \times C + (-15.4673)) \quad (8)$$

$$Y8 = \text{Tansig}(1.5396 \times A + (1.3974) \times B + (-0.0858) \times C + (-0.6297)) \quad (9)$$

$$Y9 = \text{Tansig}(-15.6196 \times A + (-0.3360) \times B + (0.2663) \times C + (-6.2506)) \quad (10)$$

$$Y10 = \text{Tansig}(-3.9240 \times A + (-0.0452) \times B + (-0.6381) \times C + (-0.5206)) \quad (11)$$

$$Y11 = \text{Tansig}(-1.4065 \times A + (-0.1150) \times B + (0.0230) \times C + (-1.1835)) \quad (12)$$

$$Y12 = \text{Tansig}(-0.9161 \times A + (0.2858) \times B + (0.3287) \times C + (0.3103)) \quad (13)$$

where in Eqs. 2 to 13, the letters A to H are as follows:

A time (s), *B* friction angle, *C* dilation angle, *D* unit weight (kN/m^3), *E* elastic modulus (kPa), *F* Poisson's ratio (v), *G* EA, and *H* EI.

5 Conclusions

In the present study, the main objective was to find a reliable predictive method to estimate the horizontal displacement of short building subjected to a Chi-Chi 1999 earthquake. Therefore, results from a total of 10,395 FEM simulations were used as the input database. After presenting the applied solutions in this study, the obtained results from each technique compared and evaluated the effect of each influential parameter. To measure the applicability of the presented technique, we used two different ranking systems. Note that the results from developed networks provided for both testing and training datasets. The obtained results proved that both proposed models have acceptable approximation results in estimation U_x with time. However, the hybrid PSO-ANN model can present as a better and more reliable ANN model in this field. The learning process was acceptable in both predictive models. In the ANN predictive model, the R^2, RMSE, and VAF for both of the training and testing datasets were (0.99961, 0.01815 and 99.713) and (0.99963, 0.01748 and 99.720), respectively, while values of (0.9997, 0.0170 and 99.9293) and (0.9997, 0.0168 and 99.9950), respectively, were obtained for training and testing of the optimized PSO-ANN predictive models. From both presented models, i.e., to estimate the horizontal deformation of short structures subjected to massive ground motion such as Chi-Chi 1999 earthquake, the PSO-ANN predictive model can provide higher performance result (e.g., lower RMSE and higher R^2 and VAF) in terms of all statistical indices for both training and testing phases compared to ANN method.

Compliance with ethical standards

Conflict of interest All the authors declare that they have no conflict of interest.

References

1. Moayedi H, Nazir R, Ghareh S, Sobhanmanesh A, Tan YC (2018) Performance analysis of piled-raft foundation system of varying pile lengths in controlling angular distortion. Soil Mech Found Eng 55:265–269
2. Kthatir A, Tehami M, Khatir S, Wahab MA (2018) Republished Paper. Multiple damage detection and localization in beam-like and complex structures using co-ordinate modal assurance criterion combined with firefly and genetic algorithms (Reprinted from Jounral of Vibroengineering 18:5063–5073 2016). J VibroEng 20:832–842
3. Dieu Tien B, Viet-Ha N, Nhat-Duc H (2018) Prediction of soil compression coefficient for urban housing project using novel integration machine learning approach of swarm intelligence and multi-layer perceptron neural network. Adv Eng Inform 38:593–604
4. Yaseen ZM, Karami H, Ehteram M, Mohd NS, Mousavi SF, Hin LS, Kisi O, Farzin S, Kim S, El-Shafie A (2018) Optimization of reservoir operation using new hybrid algorithm. KSCE J Civil Eng 22:4668–4680
5. Qin S, Zhou Y-L, Cao H, Wahab MA (2018) Model updating in complex bridge structures using kriging model ensemble with genetic algorithm. KSCE J Civil Eng 22:3567–3578
6. Jonbi J, Arini RN, Anwar B, Fulazzaky MA (2018) Effect of added the polycarboxylate ether on slump retention and compressive strength of the high-performance concrete. In: Hajek P, Han AL, Kristiawan S, Chan WT, Ismail MB, Gan BS, Sriravindrarajah R, Hidayat BA (eds) 4th international conference on rehabilitation and maintenance in civil engineering
7. Nguyen H, Bui X-N (2018) Predicting blast-induced air overpressure: a robust artificial intelligence system based on artificial neural networks and random forest. Nat Resour Res 29:1–15
8. Nguyen H, Bui X-N, Bui H-B, Mai N-L (2018) A comparative study of artificial neural networks in predicting blast-induced air-blast overpressure at Deo Nai open-pit coal mine. Vietnam. Neural Comput Appl 31:1–17
9. Bui X-N, Nguyen H, Le H-A, Bui H-B, Do N-H (2019) Prediction of blast-induced air over-pressure in open-pit mine: assessment of different artificial intelligence techniques. Nat Resour Res 29:1–21
10. Nguyen H, Bui X-N, Tran Q-H, Le T-Q, Do N-H (2019) Evaluating and predicting blast-induced ground vibration in open-cast mine using ANN: a case study in Vietnam. SN Appl Sci, 1:125
11. Nguyen H, Bui X-N, Tran Q-H, Mai N-L (2019) A new soft computing model for estimating and controlling blast-produced ground vibration based on hierarchical K-means clustering and cubist algorithms. Appl Soft Comput 77:376–386
12. Pham BT, Nguyen MD, Bui KTT, Prakash I, Chapi K, Bui DT (2019) A novel artificial intelligence approach based on multi-layer perceptron neural network and biogeography-based optimization for predicting coefficient of consolidation of soil. Catena 173:302–311
13. Nhat-Duc H, Quoc-Lam N, Dieu Tien B (2018) Image processing-based classification of asphalt pavement cracks using support vector machine optimized by artificial bee colony. J. Comput. Civ. Eng 32(5):04018037
14. Nguyen-Thoi T, Tran-Viet A, Nguyen-Minh N, Vo-Duy T, Ho-Huu V (2018) A combination of damage locating vector method (DLV) and differential evolution algorithm (DE) for structural damage assessment. Front Struct Civil Eng 12:92–108
15. Lacy SJ, Prevost JH (1987) Nonlinear seismic response analysis of earth dams. Soil Dyn Earthq Eng 6:48–63
16. Mosallanezhad M, Moayedi H (2017) Comparison analysis of bearing capacity approaches for the strip footing on layered soils. Arab J Sci Eng 42(9):3711–3722
17. Hajikhodaverdikhana P, Nazari M, Mohsenizadeh M, Shamshirband S, Chau K-W (2018) Earthquake prediction with meteorological data by particle filter-based support vector regression. Eng Appl Comput Fluid Mech 12:679–688
18. Men F (2002) Investigation of earthquake mechanisms and their impact on certain basic concepts in earthquake engineering and seismology. Earthq Eng Eng Vib 1:281–291
19. Arulmoli K, Martin GR, Gasparro MG, Shahrestani S, Buzzoni G (2004) Design of pile foundations for liquefaction-induced lateral spread displacements. Amer Soc Civil Engineers, New York
20. Gulkan P, Yazgan U (2005) Raised drift demands for framed buildings during near-field earthquakes. In: Gulkan P, Anderson JG (eds) Directions in strong motion instrumentation. Springer, Dordrecht, pp 61–81
21. Qu HL, Li RF, Hu HG, Jia HY, Zhang JJ (2016) An approach of seismic design for sheet pile retaining wall based on capacity spectrum method. Geomech Eng 11:309–323

22. Thomas S, Pillai GN, Pal K, Jagtap P (2016) Prediction of ground motion parameters using randomized ANFIS (RANFIS). Appl Soft Comput 40:624–634
23. Funck T, Dickmann T, Rihm R, Krastel S, LykkeAndersen H, Schmincke HU (1996) Reflection seismic investigations in the volcaniclastic apron of Gran Canaria and implications for its volcanic evolution. Geophys J Int 125:519–536
24. Pijush S (2010) Support vector machine for evaluating seismic liquefaction potential using standard penetration test. Disaster Adv 3:20–25
25. Latifi N, Vahedifard F, Ghazanfari E, Horpibulsuk S, Marto A, Williams J (2017) Sustainable improvement of clays using low-carbon nontraditional additive. Int J Geomech 18:04017162
26. Uncuoglu E (2015) The bearing capacity of square footings on a sand layer overlying clay. Geomech Eng 9:287–311
27. Ahmadi MM, Kouchaki BM (2016) New and simple equations for ultimate bearing capacity of strip footings on two-layered clays: numerical study. Int J Geomech 16:11
28. Gao W, Guirao JLG, Abdel-Aty M, Xi W (2019) An independent set degree condition for fractional critical deleted graphs. Discret Contin Dyn Syst-S 12:877–886
29. Gao W, Wu H, Siddiqui MK, Baig AQ (2018) Study of biological networks using graph theory. Saudi J Biol Sci 25:1212–1219
30. Gao W, Wang W, Dimitrov D, Wang Y (2018) Nano properties analysis via fourth multiplicative ABC indicator calculating. Arab J Chem 11:793–801
31. Nguyen H, Bui X-N, Bui H-B, Cuong DT (2019) Developing an XGBoost model to predict blast-induced peak particle velocity in an open-pit mine: a case study. Acta Geophys 67:1–14
32. Muthusamy S, Manickam LP, Murugesan V, Muthukumaran C, Pugazhendhi A (2019) Pectin extraction from *Helianthus annuus* (sunflower) heads using RSM and ANN modelling by a genetic algorithm approach. Int J Biol Macromol 124:750–758
33. Safaei MR, Karimipour A, Abdollahi A, Truong Khang N (2018) The investigation of thermal radiation and free convection heat transfer mechanisms of nanofluid inside a shallow cavity by lattice Boltzmann method. Phys A-Stat Mech Appl 509:515–535
34. Karimipour A, D'Orazio A, Goodarzi M (2018) Develop the lattice Boltzmann method to simulate the slip velocity and temperature domain of buoyancy forces of FMWCNT nanoparticles in water through a micro flow imposed to the specified heat flux. Phys A-Stat Mech Appl 509:729–745
35. Goodarzi M, D'Orazio A, Keshavarzi A, Mousavi S, Karimipour A (2018) Develop the nano scale method of lattice Boltzmann to predict the fluid flow and heat transfer of air in the inclined lid driven cavity with a large heat source inside, two case studies: pure natural convection & mixed convection. Phys A-Stat Mech Appl 509:210–233
36. Alrashed AAAA, Karimipour A, Bagherzadeh SA, Safaei MR, Afrand M (2018) Electro- and thermophysical properties of water-based nanofluids containing copper ferrite nanoparticles coated with silica: experimental data, modeling through enhanced ANN and curve fitting. Int J Heat Mass Transf 127:925–935
37. Asadizadeh M, Hossaini MF (2016) Predicting rock mass deformation modulus by artificial intelligence approach based on dilatometer tests. Arab J Geosci 9:15
38. Hasanzadehshooiili H, Mahinroosta R, Lakirouhani A, Oshtaghi V (2014) Using artificial neural network (ANN) in prediction of collapse settlements of sandy gravels. Arab J Geosci 7:2303–2314
39. Gao W, He TY (2017) Displacement prediction in geotechnical engineering based on evolutionary neural network. Geomech Eng 13:845–860
40. Nazir R, Moayedi H, Subramaniam P, Gue S-S (2017) Application and design of transition piled embankment with surcharged prefabricated vertical drain intersection.over soft ground. Arab J Sci Eng 43(4):1573–1582
41. Nazir R, Moayedi H, Subramaniam P, Ghareh S (2017) Ground improvement using SPVD and RPE. Arab J Geosci 10:515
42. Moayedi H, Nazir R (2017) Malaysian experiences of peat stabilization, State of the Art. Geotech Geol Eng 36(1):1–11
43. Moayedi H, Mosallanezhad M, Nazir R (2017) Evaluation of maintained load test (MLT) and pile driving analyzer (PDA) in measuring bearing capacity of driven reinforced concrete piles. Soil Mech Found Eng 54:150–154
44. Moayedi H, Mosallanezhad M (2017) Uplift resistance of belled and multi-belled piles in loose sand. Measurement 109:346–353
45. Moayedi H, Mosallanezhad M (2017) Physico-chemical and shrinkage properties of highly organic soil treated with non-traditional additives. Geotech Geol Eng 35:1–11
46. Nazir R, Moayedi H, Noor RBM, Ghareh S (2016) Development of new attenuation equation for subduction mechanisms in Malaysia water. Arab J Geosci 9:741
47. Nazir R, Ghareh S, Mosallanezhad M, Moayedi H (2016) The influence of rainfall intensity on soil loss mass from cellular confined slopes. Measurement 81:13–25
48. Nazir R, Moayedi H, Mosallanezhad M, Tourtiz A (2015) Appraisal of reliable skin friction variation in a bored pile. Proc Inst Civil Eng-Geotech Eng 168:75–86
49. Moayedi H, Nazir R, Mosallanezhad M (2015) Determination of reliable stress and strain distributions along bored piles. Soil Mech Found Eng 51:285–291
50. Kassim KA, Rashid ASA, Kueh ABH, Yah CS, Siang LC, Noor NM, Moayedi H (2015) Development of rapid consolidation equipment for cohesive soil. Geotech Geol Eng 33:167–174
51. Nazir R, Moayedi H, Pratikso A, Mosallanezhad M (2014) The uplift load capacity of an enlarged base pier embedded in dry sand. Arab J Geosci 1–12
52. Moayedi H, Nazir R, Kazemian S, Huat BK (2014) Microstructure analysis of electrokinetically stabilized peat. Measurement 48:187–194
53. Moayedi H, Nazir R, Kassim KA, Huat BK (2014) Measurement of the electrokinetic properties of peats treated with chemical solutions. Measurement 49:289–295
54. Moayedi H, Mosallanezhad M, Nazir R, Kazemian S, Huat BK (2014) Peaty soil improvement by using cationic reagent grout and electrokintic method. Geotech Geol Eng 32:933–947
55. Chang MH, Kuo CP, Shau SH, Hsu RE (2011) Comparison of SPT-N-based analysis methods in evaluation of liquefaction potential during the 1999 Chi-chi earthquake in Taiwan. Comput Geotech 38:393–406
56. Gao W, Guirao JLG, Basavanagoud B, Wu J (2018) Partial multi-dividing ontology learning algorithm. Inf Sci 467:35–58
57. Gao W, Dimitrov D, Abdo H (2018) Tight independent set neighborhood union condition for fractional critical deleted graphs and ID deleted graphs. Discret Contin Dyn Syst 12(4&5):711–721
58. Asadi A, Moayedi H, Huat BBK, Parsaie A, Taha MR (2011) Artificial neural networks approach for electrochemical resistivity of highly organic soil. Int J Electrochem Sci 6:1135–1145
59. Asadi A, Moayedi H, Huat BBK, Boroujeni FZ, Parsaie A, Sojoudi S (2011) Prediction of zeta potential for tropical peat in the presence of different cations using artificial neural networks. Int J Electrochem Sci 6:1146–1158
60. Moayedi H, Raftari M, Sharifi A, Jusoh WAW, Rashid ASA (2019) Optimization of ANFIS with GA and PSO estimating α ratio in driven piles. Eng Comput 36:1–12
61. Alnaqi AA, Moayedi H, Shahsavar A, Nguyen TK (2019) Prediction of energetic performance of a building integrated photovoltaic/thermal system thorough artificial neural network and hybrid particle swarm optimization models. Energy Convers Manag 183:137–148

62. Moayedi H, Mosallanezhad M, Mehrabi M, Safuan ARA, Biswajeet P (2018) Modification of landslide susceptibility mapping using optimized PSO-ANN technique. Eng Comput 35:1–18
63. Moayedi H, Hayati S (2018) Artificial intelligence design charts for predicting friction capacity of driven pile in clay. Neural Comput Appl 31:1–17
64. Moayedi H, Hayati S (2018) Modelling and optimization of ultimate bearing capacity of strip footing near a slope by soft computing methods. Appl Soft Comput 66:208–219
65. Mosallanezhad M, Moayedi H (2017) Developing hybrid artificial neural network model for predicting uplift resistance of screw piles. Arab J Geosci 10:10
66. Moayedi H, Armaghani DJ (2017) Optimizing an ANN model with ICA for estimating bearing capacity of driven pile in cohesionless soil. Eng Comput 34(2):347–356
67. Moayedi H, Hayati S (2018) Applicability of a CPT-based neural network solution in predicting load-settlement responses of bored pile. Int. J. Geomech 18(6):06018009
68. Moayedi H, Mosallanezhad M, Mehrabi M, Safuan ARA, Biswajeet P (2018) Modification of landslide susceptibility mapping using optimized PSO-ANN technique. Eng Comput 35:1–18
69. Moayedi H, Rezaei A (2017) An artificial neural network approach for under-reamed piles subjected to uplift forces in dry sand. Neural Comput Appl 31(2):327–336